Deterministic Global Optimization of Flapping Wing Motions for Micro Air Vehicles

Journal:	*2010 AIAA ATIO/ISSMO Conference*
Manuscript ID:	Draft
Conference:	MAOC
Date Submitted by the Author:	n/a
Contact Author:	Hajj, Muhammad

SCHOLARONE™
Manuscripts

Deterministic Global Optimization of Flapping Wing Motion for Micro Air Vehicles

Mehdi Ghommem[*], Muhammad R. Hajj[*], Layne T. Watson[†], Dean T. Mook[*]
Richard D. Snyder [‡] and Philip S. Beran [‡]

The kinematics of a flapping plate is optimized by combining the unsteady vortex lattice method with a deterministic global optimization algorithm. The design parameters are the amplitudes, the mean values, the frequencies, and the phase angles of the flapping motion. The results suggest that imposing a delay between the different oscillatory motions and controlling the way through which the wing rotates at the end of each half stroke would enhance the lift generation. The use of a general unsteady numerical aerodynamic model (UVLM) and the implementation of a deterministic global optimization algorithm provide guidance and a baseline for future efforts to identify optimal stroke trajectories for micro air vehicles with higher fidelity models.

Nomenclature

Variables and Parameters

$\mathbf{V}$	velocity	γ	circulation density
xv	locations vortex points on the plate	xc	location of control points
$\mathbf{n}$	normal vector of the plate	$\mathbf{t}$	tangential vector of the plate
N	number of bound vortices	N_w	number of wake vortices
ω	frequency	ϕ	phase angle
κ	sharpness parameter	A	amplitude
Φ	velocity potential	ΔL	panel length
$\mathbf{r}$	position vector	Δt	time step
p	pressure	ρ	density
C_p	pressure coefficient	C_L	aerodynamic lift coefficient
$\overline{C_L}$	mean value of the lift coefficient	$C_{L_{RMS}}$	root mean square value of the lift coefficient

Subscripts

n	normal direction to the plate	b	bound
u	upper	l	lower
∞	freestream	w	wake
c	control point	te	trailing edge
x	x-translation degree of freedom	y	y-translation degree of freedom
θ	rotational degree of freedom	E	pitching point

Operators

[*]Department of Engineering Science and Mechanics, Virginia Polytechnic Institute and State University, Blacksburg, VA 24061, USA.

[†]Departments of Computer Science and Mathematics, Virginia Polytechnic Institute and State University, Blacksburg, VA 24061, USA.

[‡]Air Force Research Laboratory, Wright-Patterson AFB, OH 45433-7542, USA.

American Institute of Aeronautics and Astronautics

L_1, L_2, L_5, L_6 and L_7	denote the induced velocity obtained from the Biot-Savart law
L_3	represents the impact of the freestream velocity on each control point
L_4	updates the indices of the wake vortices at each time step
L_8	represents the impact of the freestream velocity on each on each wake vortex location

I. Introduction

Micro air vehicles (MAV) are small flying vehicles that are expected to operate in urban environments where they could be subjected to harsh conditions (varying turbulence and gusts). Under these conditions, MAV must be properly designed to meet some performance specifications and thereby achieve mission endurance. In particular, enhancing aerodynamic performance of flapping MAV through increasing lift is of critical importance. This force is directly related to the size of the vehicle and would strongly influence other parameters in the constraints imposed by the MAV mission. As such, there is a need to develop multifidelity analysis, modeling, and design optimization tools. Multifidelity models can be considered and used to predict the aerodynamic behavior of flapping wings within the required accuracy and computational cost.[1,2] Platzer et al.[3] presented different levels of modeling fidelity to understand and predict flapping wing mechanisms and aerodynamics. They showed a particular interest in the unsteady panel method that predicts well the aerodynamics of flapping wings and produces results showing a good match with those obtained from higher fidelity techniques, e.g., Navier-Stokes solvers, and experiments. In a recent review paper, Shyy et al.[4] presented a literature survey on the main progress in flapping wing aerodynamics and aeroelasticity. They summarized the main aerodynamic modeling approaches and the fundamental elements that need to be included in an aerodynamic model to capture the physics of flapping wings within the required accuracy.

For optimization, generic simulations that are based on sweeping a large space of parameters would require a long time. This is especially true for high fidelity simulations that are already computationally expensive for a single run. Consequently, an optimization approach that enables an efficient way to identify the optimal set of parameters yielding good performances (sufficient lift, high efficiency, ...) would be useful. Soueid et al.[5] carried out the optimization of the kinematics of a flapping airfoil by controlling the parameters of the analytical expressions governing the heave and pitch motions. Their approach is based on numerical simulations for low Reynolds number configurations to compute the gradient of a cost functional related to a measure of flapping wing performance (propulsive efficiency, lift, ...). Chabalko et al.[6] studied an optimized stroke path for a flapping wing micro air vehicle in hover. The optimization approach was limitted to single parameter variations and suggested an amplitude of rotation of 40° as an optimal configuration for simple flapping motion. Kurdi et al.[7] performed an optimization search to locate optimal stroke trajectories for a flapping wing MAV by minimizing the mechanical power under a hovering lift constraint. The aerodynamic forces were computed from a two-dimensional quasisteady model and a gradient-based optimization approach was followed. In a recent paper, Stanford and Beran[8] performed a design optimization of a flapping wing in forward flight with a gradient-based approach. The goal of their study was maximizing the propulsive efficiency under lift and thrust constraints by changing the shape of the wing. They found that providing the wing morphing more flexibility (greater degree of spatial and temporal freedom) improves the design of a flapping wing and leads to higher efficiencies.

In this effort, we perform an efficient search for the optimal configuration for the kinematics of a flapping wing that maximizes the lift force on the flat plate. The aerodynamic model is based on the unsteady vortex lattice method (UVLM). Unlike direct numerical simulation (DNS) methods that are very expensive in terms of computational ressources, UVLM presents a good compromise between computational cost and fidelity. Then, we combine this aerodynamic tool with a deterministic global optimization algorithm VTdirect to allow for a global search of stroke paths and avoid being trapped at local maximum points.

II. Flapping Wing Kinematics

Through a cycle, the motion of the flapping wing can be defined by a combination of translations and angular oscillations. In this work, the flapping motion is based on trigonometric functions; that is, translations

and a rotation that are described by[6]

$$
\begin{aligned}
\delta_x(t) &= M_x + A_x \sin(2\pi\omega_x t + \phi_x), \\
\delta_y(t) &= M_y + A_y \sin(2\pi\omega_y t + \phi_y), \\
\theta(t) &= M_\theta + A_\theta \frac{\tan^{-1}[\kappa \sin(2\pi\omega_\theta t + \phi_\theta)]}{\tan^{-1}(\kappa)} + \frac{\pi}{2}.
\end{aligned} \tag{1}
$$

The translation motion consists of two half-strokes: the downstroke and the upstroke. At the end of each half-stroke, the rotational motion causes the plate to change its direction for the subsequent half-stroke. As defined above, the resulting stroke pattern involves thirteen control parameters including mean values, amplitudes, frequencies, and phase angles. The parameter κ represents the flipping of the plate between positive and negative inclinations at the ends of the flapping cycle. The velocity at a point P of the plate due to the flapping motion in the inertial reference frame is written as

$$
\mathbf{u}_p(d) = \left(\dot{\delta}_x - d\,\dot{\theta}\,\sin(\theta)\right)\mathbf{i} + \left(\dot{\delta}_y + d\,\dot{\theta}\,\cos(\theta)\right)\mathbf{j},
$$

where d is the distance between the point P and the pitching center E.

III.   UVLM Implementation

A.   Formulation

The unsteady flow around a flat-plate airfoil is modeled using a two-dimensional unsteady vortex lattice method (UVLM). This method has been used extensively to determine aerodynamic loads and aeroelastic responses.[9–11] For instance, Nuhait and Mook[11] implemented an aeroelastic numerical model based on a two-dimensional vortex lattice method to compute the unsteady aerodynamic loads of a flat plate in a uniform flow and predict the flutter boundary. Their prediction for the flutter speed showed an excellent agreement with the one obtained based on Theodorsen's method. In this method, it is assumed that the flow field is inviscid everywhere except in the boundary layers and the wake. A set of discrete vortices are placed on the plate to represent a viscous shear layer in the limit of the infinite Reynolds number. In this numerical model, the position of, and the distribution of vorticity in the wake, and the distribution of circulation on the plate are unknowns. The plate is divided into N piecewise straight line segments or panels. In each panel, a point vortex with a circulation density $(\gamma_b)_i(t)$ is placed at the one-quarter chord position. The no-penetration condition is imposed at the three-quarter chord position, called the control point. Figure 1 shows a schematic of the flat plate with panels, each of them having a concentrated vortex located at $xv(i)$, and a control point located at $xc(i)$. As shown in Figure 1 two coordinate systems are introduced to describe the motion of the plate: an inertial reference frame (X, Y) and a body-fixed frame (x, y). The body is assumed to translate along two directions and rotate about a pitch point E. In this work, this point is located at one half of the chord length.

The basic tool in this method is the Biot-Savart law, which gives the velocity $\mathbf{V}$ at a point $\mathbf{r}$ due to an individual vortex point located at $\mathbf{r}_0$ that has a circulation $\gamma(t)$:

$$
\mathbf{V}(\mathbf{r}, t) = -\frac{1}{2\pi}\mathbf{e}_z \times \gamma(t)\frac{\mathbf{r} - \mathbf{r}_0}{|\mathbf{r} - \mathbf{r}_0|^2}, \tag{2}
$$

where $\mathbf{e}_z$ is a unit vector perpendicular to the (x, y) plane so as to form a right-hand system with the basis vectors in the plane of the flow. Consequently, the normal component of the velocity at the control point of panel i, $xc(i)$, associated with the flow around the vortex in panel j, $xv(j)$, is

$$
\mathbf{u}_b(i, j) \cdot \mathbf{n} = u_{b_n}(i, j) = \frac{(\gamma_b)_j(t)}{2\pi}\left[\frac{1}{xv(j) - xc(i)}\right] = (\gamma_b)_j(t)L_1(i, j), \tag{3}
$$

where $\mathbf{n}$ is the normal vector of the plate. The operator L_1 is used to denote the induced velocity obtained from the Biot-Savart law. We note that for the case at hand, the plate is rigid (the relative positions of vortex and control points do not change), $L_1(i, j)$ and $\mathbf{n}(i, j)$ remain constant. The total normal component of the velocity at control point i attributed to the disturbance created by all bound vortices is then given by

$$
\left. u_{b_n}(i)\right|_{total} = \sum_{j=1}^{N} u_{b_n}(i, j) = \sum_{j=1}^{N}(\gamma_b)_j(t)L_1(i, j). \tag{4}
$$

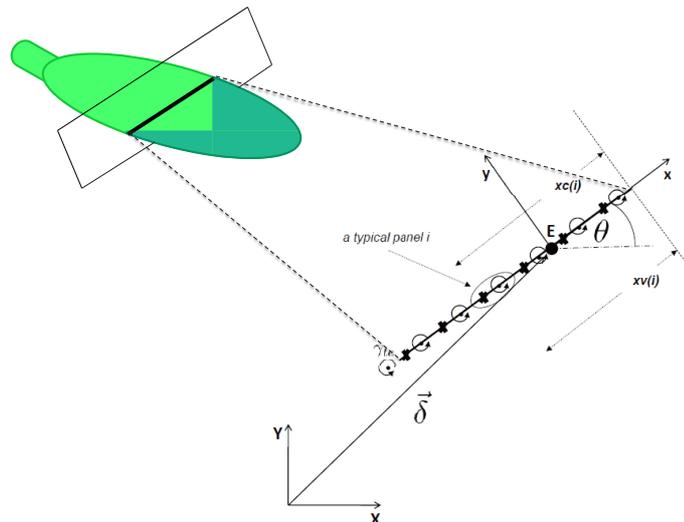American Institute of Aeronautics and Astronautics

Figure 1. Representation of a model of a flat plate with panels, each one has a concentrated vortex located at $xv(i)$**, and a control point located at** $xc(i)$**.**

B.   Wake development

In order to satisfy the Kutta condition, we force the pressure to be finite and the difference between the pressures on the upper and lower surfaces to be zero at the trailing-edge. To this end, the vorticity created at the trailing-edge is convected at local particle velocity. The wake vorticity is introduced by shedding point vortices from the trailing edge, whose circulation is denoted by $(\gamma_w)_j(t)$. These vortices are convected downstream at each time step and their positions are denoted by $(\mathbf{r}_w)_j(t)$. The induced velocity at control point i that stems from all wake vortices is given by

$$\mathbf{u}_w(i) = -\frac{1}{2\pi}\mathbf{e}_z \times \sum_{j=1}^{N_w(t)} (\gamma_w)_j(t)\frac{\mathbf{r}_{c_i} - (\mathbf{r}_w)_j}{|\mathbf{r}_{c_i} - (\mathbf{r}_w)_j|^2}, \tag{5}$$

where $\mathbf{r}_{c_i}$ is the position of the control point i in the global frame and $N_w(t)$ is the number of wake vortices. Additionally, there is the normal component of the freestream velocity, which, in this case, is the same for all control points $\mathbf{V}_\infty(t) \cdot \mathbf{n} = -L_3\mathbf{V}_\infty(t)$.

At every control point, the no-penetration condition applies and is written in the form

$$u_{b_n} = (\mathbf{u}_p - \mathbf{u}_w - \mathbf{V}_\infty) \cdot \mathbf{n}. \tag{6}$$

In terms $\gamma_b(t)$, $\mathbf{r}_w(t)$, and $\gamma_w(t)$, this condition is written as

$$L_1\gamma_b(t) = L_2\Big(\mathbf{r}_w(t)\Big)\gamma_w(t) + L_3\mathbf{V}_\infty(t), \tag{7}$$

where L_2 denotes a geometric operator that represents the induced velocity obtained form the Biot-Savart law and L_3 is an operator through which the fluctuations in the freestream velocity impact each control point.

At every time step, a vortex with circulation γ_{te} is shed from the trailing edge of the plate into the wake. The conservation of the total circulation yields

$$\sum_{i=1}^{N}(\gamma_b)_i(t) + \gamma_{te}(t) = -\sum_{j=1}^{N_w(t)}(\gamma_w)_j(t). \tag{8}$$

To render the wake force-free, vortices shed from the trailing edge retain their circulation values at all times and move with the particle velocity. Thereafter, solving Eq. (8) for given $(\gamma_b)_i(t)$ and $(\gamma_w)_j(t)$, and updating

the vector of wake vortices yields

$$(\gamma_w)_1(t+1) = \gamma_{te}(t) \tag{9}$$

and

$$(\gamma_w)_{i+1}(t+1) = (\gamma_w)_i(t), \quad \text{for} \quad i = 1, 2, ..., N_w(t). \tag{10}$$

The steps described in Eqs. (8)–(10) are then summarized as

$$\gamma_w(t+1) = L_4\gamma_w(t) + L_5\Big(\mathbf{r}_w(t)\Big)\gamma_b(t), \tag{11}$$

where L_4 is a shift operator that updates the indices of the wake vortices at each time step as a new wake vortex is shed from the trailing edge and L_5 denotes geometric operator that represents the induced velocity obtained form the Biot-Savart law.

The path of wake particles is determined using the Euler integration scheme,

$$(\mathbf{r}_w)_i(t+1) = (\mathbf{r}_w)_i(t) + \mathbf{u}_{w,i}\Big((\mathbf{r}_w)_i(t), t\Big)\Delta t, \tag{12}$$

where $(\mathbf{r}_w)_i$ is the position of a given vortex in the wake and is calculated by convecting the downstream end point of segment $i-1$ found at the previous time step and Δt is the time step. The velocity of the wake vortices $\mathbf{u}_w$ is then computed using the Biot-Savart law and combining the effects of the airfoil, the wake, and the freestream on the wake. A major problem might occur in the system of point vortices when two vortices are convected close to each other. The vortex blob concept is used to remove such a singularity. More details on this concept are provided by Pettit et al.[12] Eq. (12) is then expressed as

$$\mathbf{r}_w(t+1) = L_6\Big(\mathbf{r}_w(t)\Big)\gamma_w(t) + L_7\Big(\mathbf{r}_w(t)\Big)\gamma_b(t) + L_8\mathbf{V}_\infty(t), \tag{13}$$

where L_6 and L_7 denote geometric operators that represent the induced velocity obtained form the Biot-Savart law and L_8 is an operator through which the fluctuations in the freestream velocity are applied on each wake vortex location.

C. Aerodynamic Lift

The computation of the aerodynamic lift is performed by multiplying the difference in the pressure across each panel by its length. Using the unsteady Bernoulli equation, the difference in the pressure coefficient $C_{p_i} = (p_i - p_\infty)/(1/2\rho\overline{V}_E^2)$ across each panel i of the plate is given by

$$\Delta C_{p_i} = \left(\Big[(v_i)_u^2 - (v_i)_l^2\Big] + 2\Big[\frac{\partial\Phi_i}{\partial t}\Big|_u - \frac{\partial\Phi_i}{\partial t}\Big|_l\Big]\right), \tag{14}$$

where

$$\overline{V}_E = \frac{1}{T}\int_0^T V_E(t)\,dt.$$

Here, T is the temporal period of the prescribed oscillations of the flapping plate and V_E is the velocity of the pitching center E. The subscripts $(.)_u$ and $(.)_l$ stand for the upper and lower surfaces of the plate, respectively. The first term in Eq. 14 can be rewritten as

$$
\begin{aligned}
(v_i)_u^2 - (v_i)_l^2 &= \Big((v_i)_u + (v_i)_l\Big)\Big((v_i)_u - (v_i)_l\Big) \\
&= 2(v_i)_m\Delta v_i \\
&= 2\Big[(\mathbf{u}_w + \mathbf{u}_p)\cdot\mathbf{t}\Big]\Delta v_i, \tag{15}
\end{aligned}
$$

where $\mathbf{u}_p$ is the velocity of the plate in the inertial reference frame and $\mathbf{t}$ is the tangential vector of the plate. The velocity difference across a panel surface Δv_i is obtained by dividing the vorticity circulation strength $(\gamma_b)_i$ by the panel length $(\Delta l)_i$.

The calculation of the unsteady portion of Eq. (14) involves determining the rate of change of velocity potential Φ. The partial derivative is approximated through the first order backward difference as

$$\frac{\partial\Phi}{\partial t} \approx \frac{\Phi(r,t) - \Phi(r,t-\Delta t)}{\Delta t}. \tag{16}$$

Thus,

$$2\Big[\frac{\partial\Phi_i}{\partial t}|_u - \frac{\partial\Phi_i}{\partial t}|_l\Big] = \frac{2}{\Delta t}\Big[\Big((\Phi_i)_u(t) - (\Phi_i)_l(t)\Big) - \Big((\Phi_i)_u(t-\Delta t) - (\Phi_i)_l(t-\Delta t)\Big)\Big]. \tag{17}$$

To calculate the difference in Φ across the panel surface in Eq. (17), the definition of the velocity potential, $v = \nabla\Phi$, is manipulated to state $d\Phi = v \cdot dl$ or

$$(\Phi)_u - (\Phi)_l = \int_{l_l}^{l_u} v \cdot dl. \tag{18}$$

Because the plate is considered as a body of zero thickness, the integration of Eq. (18) is performed along a closed path. Using the definition of circulation,

$$\gamma = \oint_c v \cdot dl, \tag{19}$$

the value of the integral of Eq 18 is equal to the circulation associated with the vorticity encircled by that path. In this formulation, the circulation is simply the summation of individual strengths of vortices encountered along the path of integration. Consequently, the difference in the velocity potential is given by

$$(\Phi_i)_u(t) - (\Phi_i)_l(t) = \sum_{j=1}^{i} (\gamma_b)_j(t). \tag{20}$$

The aerodynamic lift is then calculated by integrating the pressure over the entire plate,

$$C_L(t) = \sum_{i=1}^{N}\Big[2\left[(\mathbf{u}_w + \mathbf{u}_p)\cdot \mathbf{t}\right]\frac{(\gamma_b)_i(t)}{(\Delta l)_i} + \frac{2}{\Delta t}\Big(\sum_{j=1}^{i}(\gamma_b)_j(t) - \sum_{j=1}^{i}(\gamma_b)_j(t-\Delta t)\Big)\Big]\Delta L\cos(\theta). \tag{21}$$

D.   Results

This subsection presents results of the UVLM implementation. Figure 2(a) plots the set of discrete vortices that have been shed from the trailing-edge after 10 flapping cycles. Figure 2(b) shows the corresponding instantaneous flowfield resulting from a pattern whereby the flat plate undergoes trigonometric motion at the x-translation and rotation amplitudes of $A_x = 1.0$ and $A_\theta = 40.0°$. The values of the remaining parameters are presented in Table 1. We note that this plot was generated by computing the velocity components at each point of the grid based on the Biot-Savart law. This figure shows that the flapping motion of the plate creates a downward jet of counterrotating vortices (represented by different colors). This jet-like flow feature accelerates the flow in the downward direction.

Unlike fixed-wing airplanes, insects and birds rely on the vortices created and shed by their flapping wing to generate enough lift and sustain the flight, especially when they are hovering.[1,2,4] As such, the set of counterrotating vortices shown in Figure 2(a) leads to the generation of the lift force. The time history and power spectrum of the lift on a flat plate undergoing the same trigonometric motion are plotted in Figures 3(a) and 3(b), respectively. These oscillations of the same frequency for x-translation and rotation are considered to mimic the motion of insects and birds' wings,[3,13] i.e., $\omega_x = \omega_\theta$. From Figure 3(b), we observe that the lift spectrum exhibits a peak at twice the frequency of flapping motion as well as smaller peaks at the first and third harmonics of that frequency.

IV.   Global Optimization

One important issue that should be addressed is the identification of the optimal flapping wing kinematics to meet some aerodynamic performance specifications. In this section, we combine the aerodynamic tool (UVLM) as discussed above with a deterministic global optimization algorithm (VTdirect) to determine an optimal configuration that maximizes the lift.
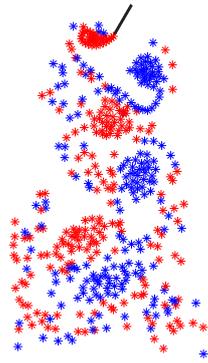
(a) Discrete vortices.
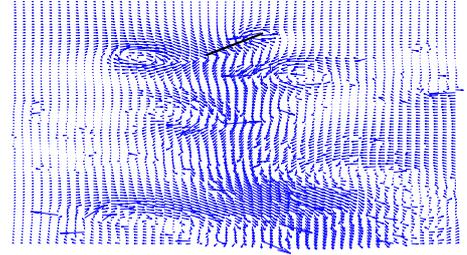
(b) Flowfield around the plate. Arrows are used to represent the velocity components at each point of the grid.

Figure 2. Flowfield for a flapping flat plate with an amplitude of rotation $A_\theta = 40.0^o$ and an amplitude of x-translation $A_x = 1.0$. The red stars represent the clockwise vortices and the blue stars represent the counter-clockwise vortices.

Table 1. Fixed Kinematics Parameters

Symbol	Description	Numerical values
y-translation amplitude	A_y	0.0
Mean value of x-translation motion	M_x	0.0
Mean value of y-translation motion	M_y	0.0
Mean value of rotational motion	M_θ	0.0
Frequency of rotation and x-translation	ω_x, ω_θ	1.0
Phase angle (x-translation)	ϕ_x	0.0
Phase angle (rotation)	ϕ_θ	$\pi/2$
Rotational sharpness	κ	3.0
Plate chord length	cl	1.0
Number of panels	N	50.0
Time step	Δt	0.02

A.   Problem formulation

MAV are usually designed to meet some performance specifications. In particular, generating enough high lift to sustain the flight is highly desirable. Here, we attempt to find a suitable kinematic configuration for the hover flight that guarantees the highest lift. To this end, we solve the global kinematic optimization problem subject to bound constraints that can be formulated as

$$\max \quad \overline{C_L}(v),$$

subject to

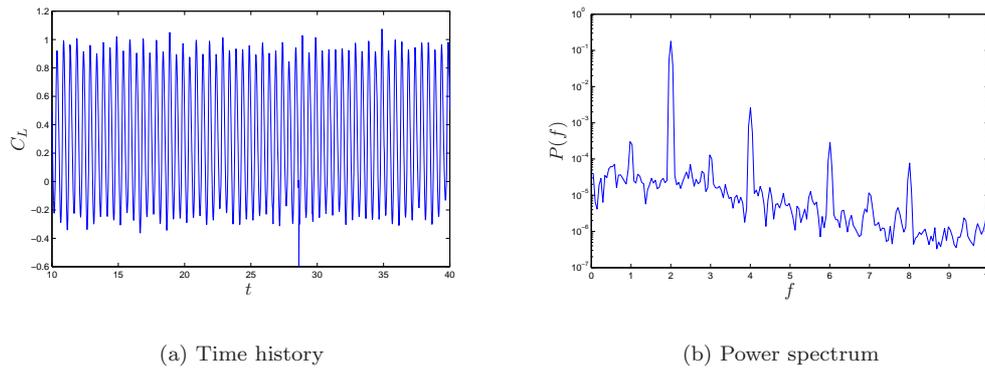$$v \in D,$$

(a) Time history　　　　　　　　　　　　(b) Power spectrum

Figure 3. Time history and power spectrum of the lift on a flat plate undergoing trigonometric motion ($A_x = 1.0$ and $A_\theta = 40.0°$).

where v is the vector of control parameters consisting of amplitudes, frequencies, mean values, and phase angles of the flapping motion, $D = \{v \in R^n \mid l \leq v \leq u\}$ is an n-dimensional bounding box, and $\overline{C_L}(v)$ is the mean value of the lift coefficient.

B.　VTdirect: global optimization algorithm

Nonlinear systems often exhibit multiple locally optimal operating points, and finding a globally optimal operating point requires global optimization. In engineering applications nondeterministic biologically inspired global search algorithms are popular, based more on the belief that evolved systems must be optimal rather than on a rigorous mathematical justification. There exist very sophisticated deterministic global search algorithms, which mounting evidence shows are usually more efficient than the nondeterministic approaches. An example of such a deterministic global optimization algorithm is the code VTdirect, a massively parallel implementation of the serial algorithm DIRECT of Jones et al.[14] The package VTDIRECT95[15] also contains a serial version VTdirect for small scale work such as is considered here. An iteration of VTdirect selects and subdivides subregions (boxes) of the feasible design space that are most likely to contain the global optimum point. Figure 4 shows the boxes produced and points sampled by VTdirect for a 2-dimensional problem over a square design space. A detailed description and analysis of the code is in He et al.[16,17] A distinctive characteristic of deterministic algorithms like VTdirect is their frugal use of function evaluations, compared to population based evolutionary algorithms (even if the latter use memory[18] and local approximations[19]).

C.　Validation: surface mapping vs. VTdirect

The optimization tool VTdirect is applied to the flapping wing whereby parameters of the flapping wing kinematics are varied. First, to check the capability of VTdirect to identify the optimal point, a parametric study, in which different configurations for ϕ_θ and A_θ are considered while keeping all other parameters fixed, is carried out. Figure 5(a) shows the variations of the mean value of the lift $\overline{C_L}$ with the phase angle ϕ_θ and the optimal points identified by VTdirect. Figure 5(b) depicts the contour plot showing the variations of the mean value of the lift $\overline{C_L}$ with the amplitude and phase angle of the rotational motion A_θ and ϕ_θ, respectively, as well as the optimal points identified by VTdirect. This surface shows local maxima in the region bounded by $40° \leq A_\theta \leq 55°$ and $115° \leq \phi_\theta \leq 125°$. As shown in Figures 5(a) and 5(b), VTdirect does a good job capturing the optimal points. We note that generating the contour plot required 1911 aerodynamic simulations while the number of function evaluations used by the run of VTdirect is only 103. Clearly, identifying the optimal configuration through sweeping the whole parameter space is inefficient. Besides, considering more parameters will add significantly to the computational cost.
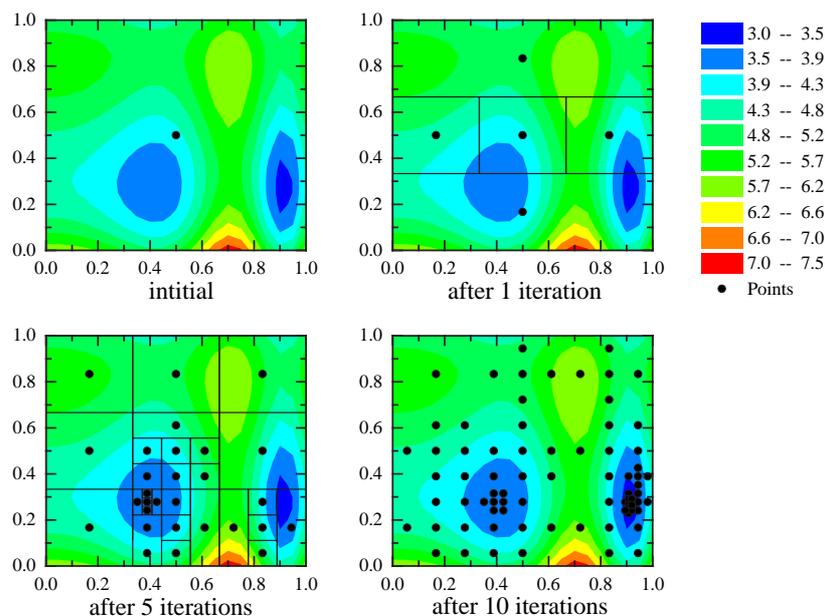
Figure 4. Boxes produced and points sampled by the serial code VTdirect for a 2-dimensional problem over a square design space.

D.   Multiparameter kinematics optimization

In this section, we consider the variation of seven parameters of the flapping wing kinematics, namely, A_x, A_y, A_θ, ϕ_x, ϕ_y, ϕ_θ, and κ. The upper and lower bounds of these parameters are presented in Table 2.

Table 2.   Control variables constraints

Parameter	Lower bound	Upper bound
A_x	1	2
A_y	0	1
A_θ	$20°$	$70°$
ϕ_x	$0°$	$360°$
ϕ_y	$0°$	$360°$
ϕ_θ	$0°$	$360°$
κ	1	4

To carry out the optimization search, stopping conditions for VTdirect were a limit number of iterations and function evaluations, minimal value for the change in the objective function, and minimum box diameter. Table 3 gives a summary of the four optimal results reported by VTdirect. We note that the number of function evaluations used by the run of VTdirect is 613. A_x, A_y, A_θ, and ϕ_y are the same for most ranges of parameters and equal to 1.018, 0.065, $61.666°$ and 354.59, respectively. Previous works[3,5] have shown that the optimum efficiency for a pitch-plunge airfoil occurs when pitch leads plunge by about $90°$. According to the results obtained from VTdirect, the performance of a flapping wing may be enhanced by considering a higher phase angle ($\phi_\theta \approx 178^o$). Figure 6 shows the flapping motion that corresponds to the optimal configuration. This flapping motion leads to a particular generation and distribution of vortices in the downward direction that maximizes the lift. We note that the numbers are introduced to show the sequence of the flapping motion.

Figure 7 shows the time history of the lift coefficient for the optimal set of kinematic parameters identified
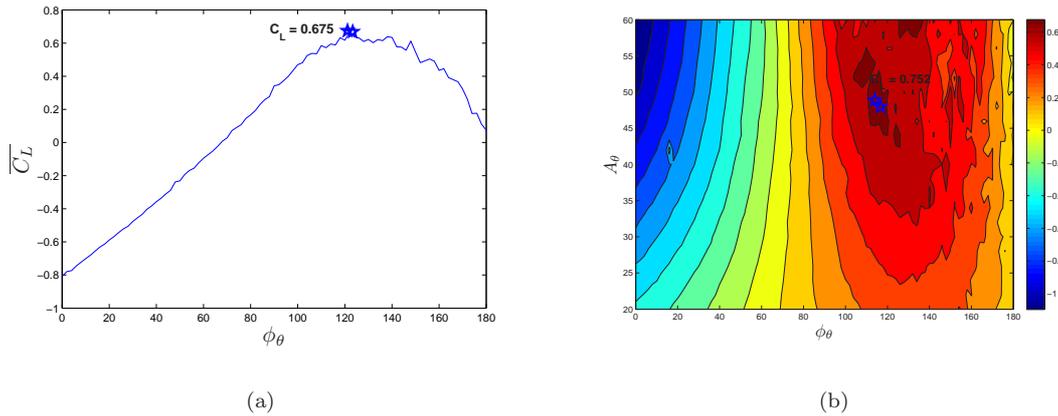
(a)   (b)

Figure 5. Variations of the mean lift $\overline{C_L}$ for a rigid flat plate: (a) with the phase angle ϕ_θ, (b) with the amplitude of rotation A_θ and phase angle ϕ_θ. The stars represent the optimal points identified by VTdirect.

Table 3. Summary of optimal configurations

Case	A_x	A_y	A_θ	ϕ_x	ϕ_y	ϕ_θ	κ	$\overline{C_L}$	$C_{L_{RMS}}$
1	1.018	0.065	61.666^o	44.159^o	354.597^o	178.333^o	1.158	**0.954**	**1.168**
2	1.018	0.064	61.666^o	37.053^o	354.597^o	178.333^o	1.158	**0.948**	**1.298**
3	1.018	0.064	61.666^o	37.053^o	354.597^o	178.333^o	1.154	**0.931**	**1.240**
4	1.018	0.064	61.666^o	37.053^o	354.597^o	177.962^o	1.154	**0.912**	**1.198**

by VTdirect. Clearly, a high value for $\overline{C_L}$ has been reached. However, the time history exhibits significant jump of the lift coefficient to relatively low negative values along a stroke cycle. Such behavior is undesirable and could affect the manoeuvrability and ability of a flapping MAV to fulfill a specific mission. To prevent this kind of behavior, we follow a penalty function approach to add a constraint to the optimization problem. The objective function (mean value of the lift coefficient) is then penalized and the optimization problem is reformulated as

$$\max \quad \left[\overline{C_L}(v) - \alpha \Big(\min_t \{C_L(t)\} - C_m \Big)_- \right],$$

subject to

$$v \in D.$$

where the penalty parameter α is set equal to 1000, C_m is the minimal allowed value of the lift coefficient, and

$$X_- = \left\{ \begin{array}{ll} -X, & X < 0 \\ 0, & X \geq 0 \end{array} \right.$$

We set C_m equal to -0.2 and carry out the reformulated optimization search. The optimal configurations are presented in Table 4. In comparison with the results obtained without penalizing the objective function, ϕ_θ and κ seem to be significant parameters that control the fluctuations of the lift force. A change in these parameters leads to a reduction in the optimal mean value of the lift coefficient while guaranteeing $C_L(t) > C_m$ all the time. Figure 8 shows a plot of the time history of the lift coefficient for the first optimal configuration reported in Table 4.

Results from the implementation of the deterministic global optimization approach with the unsteady vortex lattice method indicate that one could obtain positive benefit from a combination of the parameters
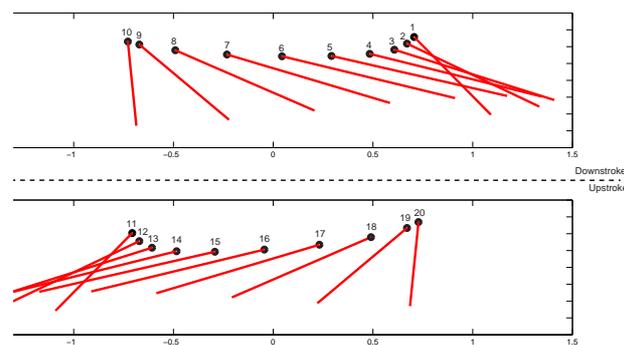
Figure 6. Half-strokes during a flapping cycle (optimal configuration). The numbers are introduced to show the sequence of the flapping motion.
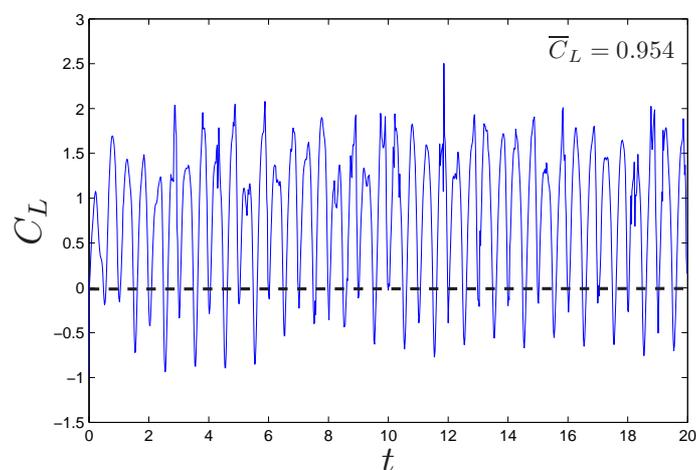

Figure 7. Time history of the lift coefficient: optimal configuration identified by VTDIRECT.

defining the flapping motion of the wing to improve the performance of its flight. As such, imposing a delay between the different oscillatory motions (by specifying appropriate phase angles of the oscillatory motions) and controlling the way through which the wing rotates at the end of each half stroke (through varying the parameter κ) might enhance the lift generation. Besides, the results obtained from the optimizer VTdirect provide guidance in how to reduce the dimensions of the design space. In fact, the low values for the amplitude of the y-translation A_y identified for the optimal configurations suggest that one could consider only the translation along the x-axis and the rotation in the flapping motion. This may be of benefit when designing the actuation mechanism. Furthermore, this would lead to a relaxation of the optimization problem and a reduction of four control parameters (M_y, A_y, ω_y, and ϕ_y). Then, we set the phases ϕ_x and ϕ_θ equal to zero and 107.8°, respectively. In other words, ϕ_θ is equal to the difference in the phases ($\phi_\theta - \phi_x$) that corresponds to the first optimal configuration reported in Table 4. Figure 9 plots the time history of the lift coefficient resulting from a pattern whereby the flat plate undergoes trigonometric motion at the x-translation and rotation amplitudes of $A_x = 1.018$ and $A_\theta = 56.042°$. The mean value of the lift fluctuations is equal to 0.687; that is, only a 3.6 % reduction in the mean value of the lift coefficient in comparison with the one identified by the optimizer VTdirect where seven design parameters have been considered. Therefore, one could further reduce the design space by setting the phase angle of the x-translation motion ϕ_x equal to zero and varying only the phase angle of the rotational motion ϕ_θ.

American Institute of Aeronautics and Astronautics

Table 4. Summary of optimal configurations (with penalty function approach)

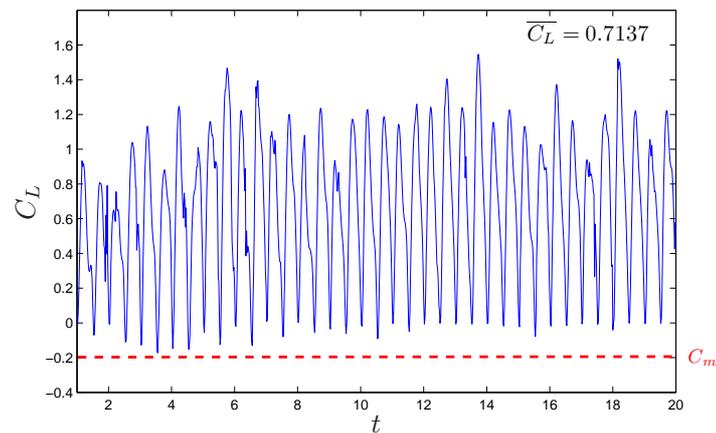| Case	A_x	A_y	A_θ	ϕ_x	ϕ_y	ϕ_θ	κ	$\overline{C_L}$	$C_{L_{RMS}}$
1	1.018	0.027	56.042^o	58.309^o	102.232^o	166.111^o	1.512	**0.7137**	**0.8268**
2	1.018	0.027	56.111^o	58.309^o	102.232^o	166.111^o	1.500	**0.7104**	**0.8166**
3	1.018	0.027	56.111^o	58.309^o	102.432^o	166.111^o	1.512	**0.7102**	**0.8412**
4	1.018	0.027	56.111^o	58.309^o	102.232^o	166.111^o	1.487	**0.7078**	**0.8180**

Figure 8. Time history of the lift coefficient: optimal configuration identified by VTDIRECT (with penalty function approach).

V.   Conclusions

In this effort, we perform an efficient search for the optimal configurations for flapping wing kinematics that maximize the lift force on the flat plate by combining the UVLM with a global optimization algorithm called VTdirect. The results suggest that imposing a delay between the different oscillatory motions and controlling the way through which the wing rotates at the end of each half-stroke would enhance the lift generation. Besides, the results obtained from the optimizer VTdirect provide guidance in how to reduce the dimensions of the design space. In fact, they indicate a possible reduction in the number of control parameters with an insignificant decrease in the lift. This may be of benefit when designing the actuation mechanism of a flapping wing.

VI.   Acknowledgments

References

[1]Mueller, T. H., *Fixed and Flapping Wing Aerodynamics for Micro Air Vehicles Applications*, American Institute of Aeronautics and Astronautics, Inc, 2001.

[2]Ansari, S. A., Zbikowski, R., and Knowles, K., "Aerodynamic Modelling of Insect-like Flapping Flight for Micro Air Vehicles," *Progress in Aerospace Sciences*, Vol. 42, 2006, pp. 129–172.

[3]Platzer, M. F. and Jones, K. D., "Flapping-Wing Aerodynamics: Progress and Challenges," *AIAA Journal*, Vol. 46,
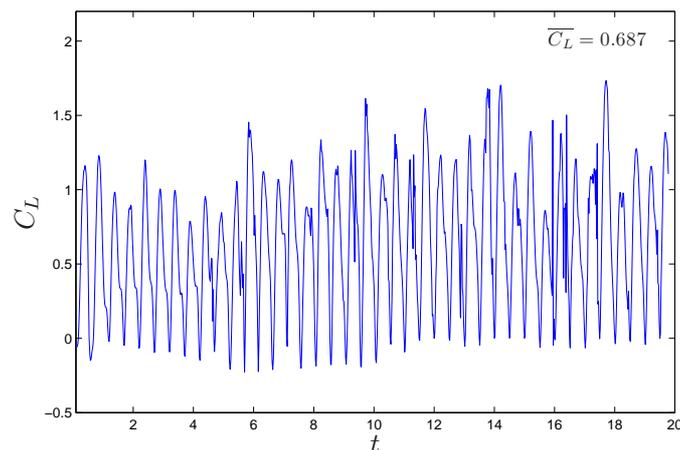
Figure 9. Time history of the lift coefficient ($A_y = 0$, $\phi_x = 0^o$, and $\phi_\theta = 107.8^o$).

2008, pp. 2136–2149.

[4]Shyy, W., Aono, H., Chimakurthi, S. K., Trizila, P., Kang, C. K., Cesnik, C. E. E., and Liu, H., "Recent progress in flapping wing aerodynamics and aeroelasticity," *Progress in Aerospace Sciences*, 2010, pp. 1–444.

[5]Soueid, H., Guglielmini, L., Airiau, C., and Bottaro, A., "Optimization of the Motion of a Flapping Airfoil Using Sensitivities Functions," *Computers and Fluids*, Vol. 38, 2009, pp. 861–874.

[6]Chabalko, C. C., Snider, R. D., Beran, P. S., and Parker, G. H., "The Physics of an Optimized Flapping Wing Micro Air Vehicle," *Proceedings of the 47th AIAA Aerospace Science Meeting Including The New Horizons Forum and Aerospace Exposition*, AIAA Paper No. 2009-801, 2009.

[7]Kurdi, M., Stanford, B., and Beran, P., "Kinematic Optimization of Insect Flight for Minimum Mechanical Power," *Proceedings of the 48th AIAA Aerospace Science Meeting Including The New Horizons Forum and Aerospace Exposition*, AIAA Paper No. 2010-1420, 2010.

[8]Stanford, B. K. and Beran, P. S., "Analytical Sensitivity Analysis of an Unsteady Vortex-Lattice Method for Flapping-Wing Optimization," *Journal of Aircraft*, Vol. 47, 2010, pp. 647–662.

[9]Wang, Z., *Time-Domain Simulations of Aerodynamic Forces on Three-Dimensional Configurations, Unstable Aeroelastic Responses, and Control by Network Systems*, Ph.D. thesis, Virginia Polytechnic Institute and State University, 2004.

[10]DeLaurier, J. and Winfield, J., "Simple Marching-Vortex Model for Two-Dimensional Unsteady Aerodynamics," *Journal of Aircraft*, Vol. 27, 1990, pp. 376–378.

[11]Nuhait, A. O. and Mook, D. T., "Aeroelastic Behavior of Flat Plates Moving Near the Ground," *Journal of Aircraft*, Vol. 47, 2010, pp. 464–474.

[12]Pettit, C., Hajj, M. R., and Beran, P. S., "Gust Loads with Uncertainty Due to Imprecise Gust Velocity Spectra," *Proceedings of the 48th AIAA/ASME/ASCE/AHS/ASC Structures, Structural Dynamics, and Materials Conference*, AIAA Paper No. 2007-1965, 2007.

[13]Shyy, W., Lian, Y., Tang, J., Liu, H., Trizila, P., Stanford, B., bernal, L., Cesnik, C., Friedmann, P., and Ifju, P., "Computational Aerodynamics of Low Reynolds Number Plunging, Pitching and Flexible Wings for MAV Applications," *Proceedings of the 46th AIAA Aerospace Science Meeting and Exhibit*, AIAA Paper No. 2008-523, 2008.

[14]Jones, D. R., Perttunen, C. D., and Stuckman, B. E., "Lipschitzian optimization without the Lipschitz constant," *The Journal of Optimization Theory and Applications*, Vol. 79, 1993, pp. 157–181.

[15]He, J., Watson, L. T., and Sosonkina, M., "Algorithm 897: VTDIRECT95: serial and parallel codes for the global optimization algorithm DIRECT," *ACM Trans. Math. Software*, Vol. 36, 2009, pp. 1–24.

[16]He, J., Verstak, A., Watson, L. T., and Sosonkina, M., "Performance modeling and analysis of a massively parallel DIRECT—Part 1," *Internat. J. High Performance Comput. Appl.*, Vol. 23, 2009, pp. 14–28.

[17]He, J., Verstak, A., Watson, L. T., and Sosonkina, M., "Performance modeling and analysis of a massively parallel DIRECT—Part 2," *Internat. J. High Performance Comput. Appl.*, Vol. 23, 2009, pp. 29–41.

[18]Kogiso, N., Watson, L. T., Gurdal, Z., Haftka, R. T., and Nagendra, S., "Design of composite laminates by a genetic algorithm with memory," *Mech. Composite Materials Structures*, Vol. 1, 1994, pp. 95–117.

[19]Nagendra, S., Jestin, D., Gurdal, Z., Haftka, R. T., and Watson, L. T., "Improved genetic algorithms for the design of stiffened composite panels," *Comput. & Structures*, Vol. 58, 1996, pp. 543–555.